IL-7R signaling in regulatory T cells of adipose tissue is essential for systemic glucose homeostasis

Shizue Tani-ichi, Shinya Abe, Hitoshi Miyachi, Satsuki Kitano, Akihiro Shimba, Aki Ejima, Takahiro Hara, Guangwei Cui, Tomonobu Kado, Shohei Hori, Kazuyuki Tobe, Koichi Ikuta

The Journal of Immunology, 2025, **00**, 1–14
https://doi.org/10.1093/jimmun/vkae064
Research Article

IL-7Rα signaling in regulatory T cells of adipose tissue is essential for systemic glucose homeostasis

Shizue Tani-ichi[1,2,*], Shinya Abe[1], Hitoshi Miyachi[3], Satsuki Kitano[3], Akihiro Shimba[1,2], Aki Ejima[1,4], Takahiro Hara[1], Guangwei Cui[1], Tomonobu Kado[5], Shohei Hori[6], Kazuyuki Tobe[7], and Koichi Ikuta[1,*]

[1]Laboratory of Immune Regulation, Department of Virus Research, Institute for Life and Medical Sciences, Kyoto University, Kyoto, Japan
[2]Department of Human Health Sciences, Graduate School of Medicine, Kyoto University, Kyoto, Japan
[3]Reproductive Engineering Team, Institute for Life and Medical Sciences, Kyoto University, Kyoto, Japan
[4]Graduate School of Biostudies, Kyoto University, Kyoto, Japan
[5]First Department of Internal Medicine, Faculty of Medicine, University of Toyama, Toyama, Japan
[6]Laboratory of Immunology and Microbiology, Graduate School of Pharmaceutical Sciences, The University of Tokyo, Tokyo, Japan
[7]Research Center for Pre-Disease Science, Faculty of Medicine, University of Toyama, Toyama, Japan

*Corresponding authors: Laboratory of Immune Regulation, Department of Virus Research, Institute for Life and Medical Sciences, Kyoto University, Kyoto 606-8507, Japan. Email: taniichi.shizue.6m@gmail.com; and Laboratory of Immune Regulation, Department of Virus Research, Institute for Life and Medical Sciences, Kyoto University, Kyoto 606-8507, Japan. Email: ikuta.koichi.6c@kyoto-u.ac.jp.

Abstract

Regulatory T cells (Tregs) mediate tissue homeostasis and repair. The function of the interleukin-7 receptor α (IL-7Rα) in nonlymphoid tissue Tregs is still unknown, although low expression of IL-7Rα is a widely accepted marker for Tregs. Here, we show that IL-33R (ST2)–expressing Tregs in the visceral adipose tissue (VAT) express the IL-7Rα at high levels. Treg-specific IL-7Rα–deficient mice exhibited reduced adipose ST2$^+$ Tregs and impaired glucose tolerance, whereas IL-7Rα was dispensable for Tregs in lymphoid tissues. Mice deficient in thymic stromal lymphopoietin (TSLP), an additional ligand for IL-7Rα, displayed a modest decrease in adipose ST2$^+$ Tregs and a reduced accumulation of adipose eosinophils, accompanied by slightly impaired glucose tolerance. In the VAT, mesothelial cells expressed IL-7, whereas adipose stem cells and folate receptor β–expressing tissue-resident macrophages expressed TSLP. Thus, this study indicates the significance of IL-7Rα signaling in the maintenance of VAT Tregs and glucose homeostasis, revealing a novel role for IL-7 and TSLP in immunometabolism.

Keywords: IL-7, TSLP, regulatory T cells, eosinophils, adipose tissue

Graphical abstract

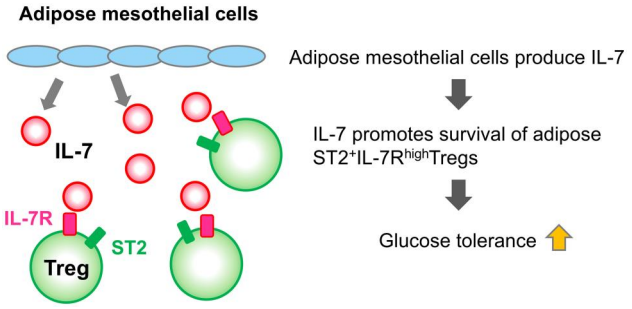

Introduction

Regulatory T cells (Tregs) suppress autoreactive immune responses and establish peripheral tolerance. Recently, Tregs have been identified in nonlymphoid tissues, such as the intestine, adipose tissue, skin, brain, skeletal muscle, and bone marrow.[1,2] DNA methylation, T cell receptor (TCR) repertoire, and transcriptome analyses have revealed that tissue Tregs have unique features and are distinct from lymphoid tissue–associated Tregs.[3–5] Expression of the interleukin (IL)-33 receptor ST2 is characteristic of tissue Tregs. ST2$^+$ Tregs play essential roles in tissue homeostasis and repair by producing the immunosuppressive cytokine IL-10 and the growth factor amphiregulin (Areg).[6–8] Tregs in visceral adipose tissue (VAT) suppress tumor necrosis factor α (TNF-α) production by M1 macrophages through IL-10, which facilitates the translocation of glucose transporter 4 to the plasma membrane and the glucose uptake of adipocytes following insulin signaling, maintaining adipose tissue homeostasis and insulin sensitivity.[9–12] In addition to Tregs, type 2 innate lymphoid cells (ILC2s) and eosinophils play essential roles in adipose tissue. ILC2s produce IL-5, which promotes eosinophil accumulation. Eosinophils produce IL-4 and induce M2

Received: December 13, 2023. **Accepted:** December 17, 2024

macrophages, which prevent inflammation-induced insulin resistance via IL-10 and arginase 1.[13,14]

IL-7 receptor α-chain (IL-7Rα) transmits signals for IL-7 and thymic stromal lymphopoietin (TSLP) by dimerization with the common γ-chain and TSLP receptor (TSLPR), respectively.[15] IL-7Rα is mainly expressed in lymphocytes. TSLP is a cytokine produced by epithelial cells, stromal cells, dendritic cells, basophils, and mast cells. Several immune cells, including dendritic cells, T cells, and ILC2s, express TSLPR.[16] IL-7 is essential for T cell development and maintenance, whereas TSLP does not affect T cell development and is involved in the progression of allergic diseases by promoting type 2 immune responses.[16,17] TSLP also plays a role in lipid metabolism.[18] TSLP stimulates T cells to migrate to the sebaceous glands of the skin and promotes sebum secretion, which causes white adipose loss and improves insulin sensitivity and steatohepatitis induced by a high-fat diet (HFD). In addition, TSLP acts as a homeostatic factor for activated Tregs in the skin.[19] Thus, IL-7Rα may mediate tissue homeostasis and allergic responses.

Low expression of IL-7Rα is characteristic of Tregs. Low IL-7Rα expression is correlated with high Foxp3 expression and suppressive function, whereas high IL-7Rα expression is consistent with conventional T cells.[20,21] Conversely, Tregs constitutively express high levels of the IL-2Rα (CD25), and IL-2 signaling plays a pivotal role in the maintenance of Tregs.[22,23] In contrast to conventional T cells, IL-7 is dispensable for Treg maintenance under IL-2 sufficient conditions.[24] However, it has been reported that IL-7Rα–deficient Tregs have weaker suppressive activity in the skin allograft rejection model.[25] Thus, whether IL-7Rα is required for the function of nonlymphoid tissue Tregs at steady state remains unclear.

To investigate the role of the IL-7Rα in tissue Tregs, we analyzed *Foxp3*$^{\text{YFP-Cre}}$ *IL7rα*$^{\text{flox/flox}}$ (IL-7R$^{\Delta\text{Treg}}$) mice. ST2^{+} effector Tregs expressed IL-7Rα at high levels. IL-7R$^{\Delta\text{Treg}}$ mice had fewer ST2^{+} Tregs in the VAT, showed impaired glucose tolerance, and developed liver steatosis on HFD. TSLP-deficient mice exhibited a modest decrease in VAT ST2^{+} Tregs and reduced eosinophil accumulation in the VAT, accompanied by slight impairment in glucose tolerance. These findings demonstrate the essential role of IL-7R signaling in the maintenance of adipose tissue Tregs and suggest a potential role for IL-7 and TSLP in glucose homeostasis, providing new insights for therapeutic intervention in type 2 diabetes.

Materials and methods

Mice

IL-7Rα–floxed mice[26] were bred with Foxp3$^{\text{YFP-Cre}}$ mice.[27] IL-7R$^{\Delta\text{Treg}}$ mice indicate Foxp3$^{\text{YFP-Cre/Y}}$ IL-7R$^{\text{fl/fl}}$ or Foxp3$^{\text{YFP-Cre/YFP-Cre}}$ IL-7R$^{\text{fl/fl}}$. Foxp3$^{\text{YFP-Cre/Y}}$ IL-7R$^{+/+}$ or Foxp3$^{\text{YFP-Cre/YFP-Cre}}$ IL-7R$^{+/+}$ mice were used as control mice. Each pair of same-sex control and knockout (KO) mice from the same litter were analyzed simultaneously, and data from multiple mixed-sex pairs from different litters were pooled. IL-7$^{\text{GFP/+}}$ mice were previously described.[28] Rag2$^{-/-}$ mice on a C57BL/6J (CD45.2) background were a kind gift from Dr. F.W. Alt (Harvard Medical School). Foxp3$^{\text{hCD2}}$-knockin mice (Foxp3$^{\text{hCD2}}$) were provided by Dr. S. Hori (University of Tokyo).[29]

TSLP-deficient (TSLP KO) mice were generated using CRISPR/Cas9/single guide RNA (sgRNA)–mediated gene editing. Two sgRNAs were designed to delete from exon 2 to intron 3. sgRNA was synthesized by Integrated DNA Technologies. The sgRNA sequences were as follows: TSLP exon 2, CTGCAAGTACTAGTACGGATGGG; and TSLP intron 3, TCCGCGGGGTGGCCCGCATCCGG. sgRNA and Cas9 protein (Thermo Fisher Scientific) were microinjected into the pronuclei of fertilized eggs obtained from the C57BL/6 mice. Tail DNA was amplified by polymerase chain reaction (PCR) with the following primers to detect the deletion of the targeted region: wild-type (WT) allele, primer 1, 5′-ACGGGAAACAGAGTTGGAAC-3′, and primer 2, 5′-CAAATCTCCAGTCAGGTCATGA-3′; KO allele, primer 1 and primer 3, 5′-GCCTATTGCAAATTGCTCC-3′. Chimeric mice were backcrossed with C57BL/6J mice for 2 to 4 generations and used for analysis. TSLP$^{-/-}$ mice were compared with sex-matched TSLP$^{+/+}$ littermates (control). All mice were maintained under specific pathogen-free conditions at the Experimental Research Center for Infectious Diseases of the Institute for Life and Medical Sciences, Kyoto University. All mouse protocols were approved by the Animal Experimentation Committee of the Institute for Life and Medical Sciences at Kyoto University.

Cell preparation

Lymph node cells were obtained from the cervical, axillary, brachial, inguinal, and mesenteric regions. VAT was isolated from the perigonadal region (epididymal in males and periovarian in females). VAT lymphocytes were isolated as previously reported, with minor modifications.[30] Briefly, perigonadal fat pads were excised after perfusion with phosphate-buffered saline (PBS), minced with scissors, and incubated for 1 h at 37 °C in 2 mL RPMI 1640 medium containing 1.25 mg/mL collagenase D (Roche), 20 μg/mL collagenase P (Roche), and 50 μg/mL DNase I (Worthington). The cell suspension was filtered through a 100 μm cell strainer and centrifuged at 440 *g* for 7 min at room temperature. The cell pellet was collected as stromal vascular fraction (SVF), and lymphocytes were enriched from SVF by centrifugation at 40% and 80% Percoll.

Antibodies and flow cytometry

The following fluorescent dye- or biotin-conjugated anti-mouse antibodies were used: CD4 (GK1.5 or RM4-5), CD8α (53-6.7), CD44 (IM7), Foxp3 (FJK-16s), ST2 (RM-ST2-2), Ki-67 (SolA15), E4BP4 (S2M-E19), rat IgG2aκ isotype control (eBR2a), mouse IgG1 isotype control (MOPC-21), and streptavidin-PE-Cy7 (all from Thermo Fisher Scientific); TCRβ (H57-597), CD3ε (145-2C11), B220 (RA3-6B2), CD11b (M1/70), CD11c (N418), Gr-1 (RB6-8C5), FcεRIα (MAR-1), NK1.1 (PK136), TER-119, Ly-6G (1A8), Siglec-F (S17007L), CD25 (PC61.5), CD45.2 (104), IL-7Rα (A7R34), IL-10 (JES5-16E3), TSLPR (22H9), PD-1 (29F.1A12), KLRG1 (2F1/KLRG1), CCR7 (4B12), IFN-γ (XMG1.2), IL-17A (TC11-18H10.1), Bcl-2 (BCL/10C4), CD31 (MEC13.3), gp38 (8.1.1), PDGFRα (APA5), IL-4 (11B11), IL-5 (TRFK5), donkey polyclonal anti-rabbit IgG (Poly4064), streptavidin-APC, streptavidin-PE, ad hamster IgG isotype control (HTK888) (all from BioLegend); CD152 (CTLA4, UC10-4F10-11), Siglec-F (E50-2440), and RORγt (Q31-378) (all from BD Biosciences); PPAR-γ (B-5) (Santa Cruz Biotechnology); and rabbit lyve-1 polyclonal antibody (ReliaTech). The lineage marker cocktail contained antibodies against CD3ε, B220, CD11b, CD11c, Gr-1, FcεRIα,

NK1.1, and TER-119. Debris and dead cells were excluded from the analysis using forward and side scatter and propidium iodide gating. Intracellular staining was performed with intracellular fixation buffer, Foxp3 staining buffer set (Thermo Fisher Scientific), or Cytofix/Cytoperm (BD Biosciences) according to the manufacturer's instructions. Stained cells were analyzed using a FACSVerse flow cytometer (BD Biosciences). Data analysis was performed using FlowJo software v9.9.6 (BD Biosciences). Cell sorting was performed using a FACSAria II or III cell sorter (BD Biosciences).

Glucose tolerance test and insulin tolerance test

Male mice 15 to 20 wk of age were used. For the glucose tolerance test (GTT), mice and their littermate controls were fasted for 16 h. The mice were then injected intraperitoneally with 2.0 g/kg of body weight of D-glucose (Nacalai Tesque) dissolved in PBS. For the insulin tolerance test, mice and their littermate controls were fasted for 3 h. The mice were injected intraperitoneally with 0.8 units/kg of body weight of insulin (Humulin R; Eli Lilly Japan) dissolved in PBS. Blood was collected from the tail tip at the indicated times, and blood glucose concentrations were measured using LaboGluco (ForaCare Japan). The area under the curve of intraperitoneal GTT and insulin tolerance test was calculated using GraphPad Prism 9 (GraphPad Software).

High-fat diets

Where indicated, 15-wk-old male mice were fed an HFD (60 kcal%, D12492; Research Diets) for 3 wk.

Histology

Tissues were excised, fixed in 10% formalin for 3 h at room temperature, and embedded in paraffin. Tissues were cut into 5 μm sections and stained with hematoxylin and eosin (Muto Pure Chemicals). Images were captured using a BZ-X810 microscope (Keyence).

Serum and hepatic lipid measurements

For blood triglyceride and total cholesterol measurements in normal diet-fed mice, mice were fasted for 16 h and then fed a standard diet for 6 h. Blood was collected from the abdominal aorta immediately after euthanasia. For low-density lipoprotein (LDL) cholesterol measurements in HFD-fed mice, blood was collected from the abdominal aorta immediately after euthanasia. The samples were centrifuged, and the supernatants were collected. Liver homogenates from HFD-fed mice were prepared as described previously.[18] Triglyceride, total cholesterol, and LDL cholesterol levels were measured by Oriental Yeast.

Cell culture

Cells were cultured in RPMI 1640 (Nacalai Tesque) medium supplemented with 10% fetal calf serum, 50 μM 2-ME, and penicillin/streptomycin containing 50 ng/mL PMA (Cayman Chemical), 500 ng/mL ionomycin (Cayman Chemical), and 10 μg/mL brefeldin A (Cayman Chemical) at 37 °C and 5% CO_2 for 4 h. Where indicated, cells were cultured with recombinant mouse IL-7 (20 ng/mL; BioLegend) or TSLP (100 ng/mL; eBioscience) for 21 h.

Dextran sulfate sodium–induced colitis

Mice were given 3% dextran sulfate sodium (DSS) (molecular weight 36–50 kDa; MP Biomedicals) in drinking water for 7 d. Body weight, stool consistency, and fecal blood were monitored daily. Disease activity index scoring was performed as previously described.[31]

Quantitative real-time PCR

WT and TSLP KO mice received 100 μg papain (Sigma-Aldrich) intranasally. After 18 h, the lungs were homogenized using Sepasol-RNA I Super-G (Nacalai Tesque), and total RNA was isolated. Complementary DNA was synthesized with a random primer (Thermo Fisher Scientific) using ReverTra Ace (TOYOBO). Quantitative real-time PCR was performed using the StepOnePlus Real-Time PCR System (Thermo Fisher Scientific) and TB Green Premix Ex Taq II (Takara). StepOne software v2.3 (Thermo Fisher Scientific) was used to analyze the data. The primers used were as follows: HPRT,[32] TSLP, 5′-CGACAGCATGGTTCTTCTCA-3′ (primer 4 in Fig. S4B), and 5′-CGATTTGCTCGAACTTAGCC-3′ (primer 5 in Fig. S4B).

Enzyme-linked immunosorbent assay

WT and TSLP KO mice were given 100 μg of papain intranasally (Sigma-Aldrich). After 18 h, the lungs were harvested and homogenized in 0.5 mL lysis buffer (0.5% Triton X-100, 150 mM NaCl, 15 mM Tris (pH 7.4), 1 mM $CaCl_2$, 1 mM $MgCl_2$, and protease inhibitor). The homogenates were centrifuged at 10,000 *g* for 10 min. According to the manufacturer's instructions, 100 μL of the supernatant was analyzed for TSLP using the DuoSet ELISA kit (R&D Systems).

Single-cell RNA sequencing analysis

Single-cell RNA sequencing (scRNA-seq) data of hematopoietic lineage marker (CD5, CD45R [B220], CD11b, Gr-1 [Ly-6G/C], 7/4, and Ter-119) positive and negative cells isolated from the SVF of epididymal white adipose tissue of C57BL/6J mice (male, 8–9 wk old) were downloaded from the Sequence Read Archive (SRP145475; https://www.ncbi.nlm.nih.gov/sra/).[33] Fastq files were processed using the Cell Ranger pipeline (v.6.1.1) with default parameters (https://support.10xgenomics.com/single-cell-gene-expression/software/pipelines/latest/what-is-cell-ranger) (processed by Takara Bio analysis service). Refdata-gex-mm10-2020-A was used as the reference. Chemistry was set to SC3Pv2. Clustering and gene expression of the Cell Ranger output were visualized using 10x Genomics Loupe Browser (v.7.0.1) (https://support.10xgenomics.com/single-cell-gene-expression/software/visualization/latest/what-is-loupe-cell-browser). The following marker genes were used for cluster annotation[34]: adipocyte, *Adipoq*; ASPC, *Pdgfra*; mesothelial, *Msln*; endothelial, *Jam2*; lymphatic endothelial, *Prox1*; macrophage, *Mafb*; monocyte, *Cybb*; dendritic cell, *Flt3*; neutrophil, *Csf3r*; B cell, *Ms4a1*; T cell, *Cd3d*; and ILC2, *Il1rl1*.

Intracellular staining of IL-7^{GFP}

A modified intracellular staining procedure was used.[35] SVF from perigonadal adipose tissue of 15-wk-old male mice was prepared as described in Cell Preparation and incubated with TruStain FcX (anti-CD16/32, Fc receptor blocking antibody) (BioLegend). After cell surface staining, cells were fixed with 0.5% paraformaldehyde on ice for 30 min and washed. Cells were then fixed and permeabilized with Fixation/Permeabilization Solution (BD Biosciences) for 30 min on ice. Cells were washed with Perm/Wash Buffer (BD Biosciences) and incubated with Alexa Fluor 488 anti-GFP polyclonal

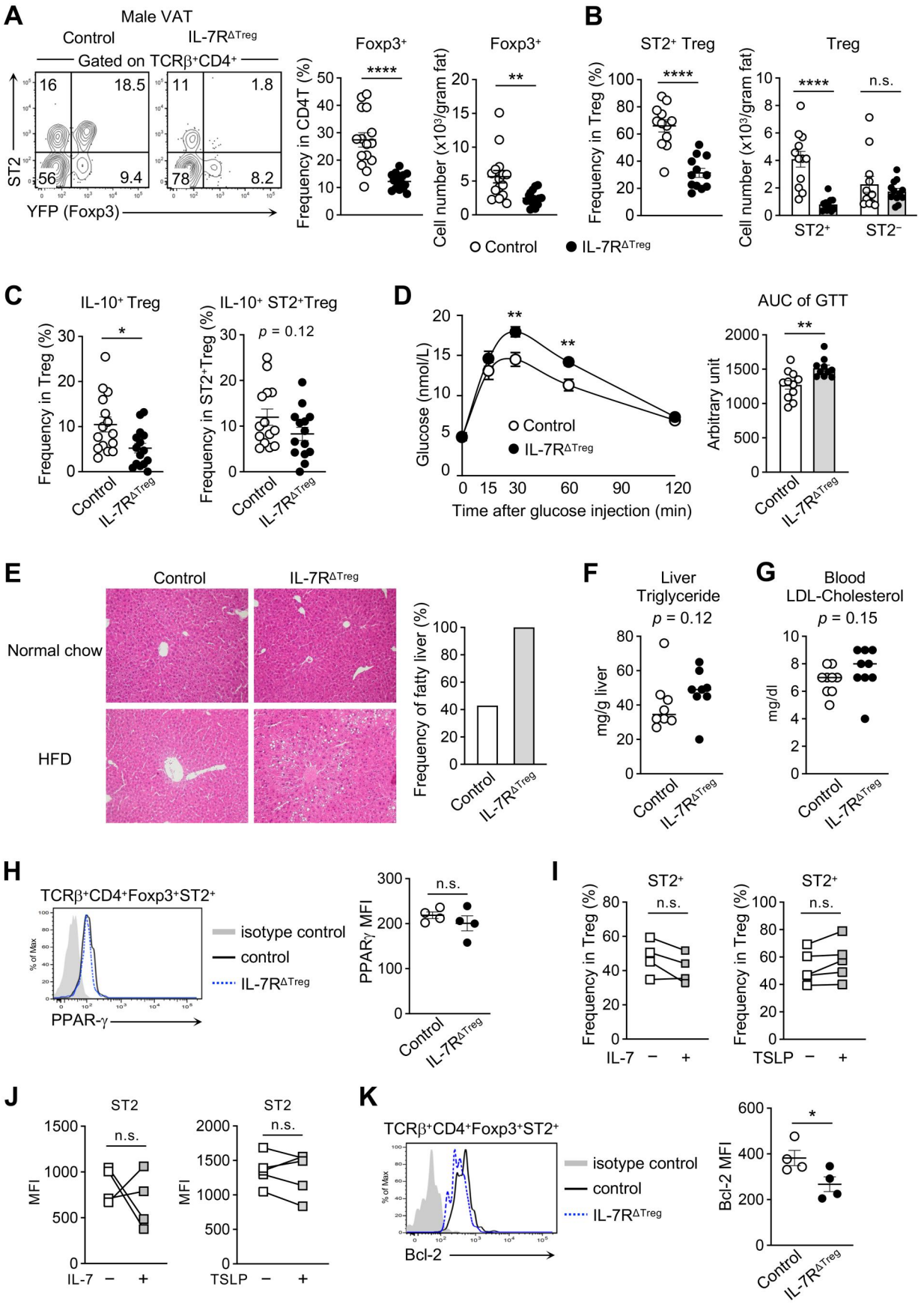

Figure 1. Impaired glucose tolerance in IL-7R$^{\Delta Treg}$ mice. (A) Flow cytometric analysis of VAT Tregs from control and IL-7R$^{\Delta Treg}$ male mice at 15 wk of age. The numbers in each panel indicate the percentage of gated populations. Graphs show the frequency of Tregs among VAT CD4 T cells and the number of VAT Tregs (n = 15 mice per group). (B) Frequency of ST2^{+} Tregs among VAT Tregs and number of ST2^{+} and ST2^{-} VAT Tregs in 15-wk-old male mice (n = 12 mice per group). (C) Frequency of IL-10–producing VAT Tregs. VAT lymphocytes were stimulated with PMA and ionomycin for 4 h. Frequency of

(Continued)

Figure 1. Continued
IL-10$^+$ Tregs was determined by gating the TCRβ$^+$CD4$^+$Foxp3$^+$ or TCRβ$^+$CD4$^+$Foxp3$^+$ST2$^+$ populations (n = 14–15 mice per group). (D) GTT was performed on control and IL-7R$^{\Delta Treg}$ mice at 15 wk of age (n = 10–11 mice per group). The bar graph indicates the area under the curve (AUC) of GTT calculated using GraphPad Prism. (E) Representative images of hematoxylin and eosin–stained liver sections from the indicated mice 3 wk after feeding the standard diet and HFD. The graph indicates the frequency of mice in the HFD-fed groups with lipid droplets in the liver (n = 7 mice per group). (F) Liver triglyceride levels in control and IL-7R$^{\Delta Treg}$ male mice fed an HFD for 3 wk (n = 8 mice per group). (G) Blood LDL cholesterol in control and IL-7R$^{\Delta Treg}$ male mice fed an HFD for 3 wk (n = 9 mice per group). (H) Flow cytometric analysis of intracellular PPARγ expression in VAT ST2$^+$ Tregs. Data represent 3 independent experiments (n = 4 mice per group). The graph shows the mean fluorescence intensity (MFI) of PPARγ. (I, J) VAT lymphocytes from *Foxp3*$^{YFP\text{-}Cre}$ and *Foxp3*^{hCD2} mice were cultured for 21 h in the presence or absence of IL-7 or TSLP. Frequency of ST2$^+$ cells in VAT Tregs (I) and the MFI of ST2 (J) were determined by gating on TCRβ$^+$CD4$^+$YFP(Foxp3)$^+$ or TCRβ$^+$CD4$^+$hCD2(Foxp3)$^+$. Data are from 3 independent experiments (IL-7, n = 4 mice per group; TSLP, n = 5 mice per group). (K) Bcl-2 expression in ST2$^+$ Tregs in the VAT. Shown represents 4 independent experiments, and the graph summarizes the MFI of Bcl-2. (A–D, H, K) Data are mean ± SEM. Statistics were performed using unpaired *t* tests. (I, J) A paired 2-tailed Student's *t*-test was used. *$P < 0.05$, **$P < 0.01$, ****$P < 0.0001$. (F, G) Bars indicate the median of each group. The *P* value was measured using the Mann-Whitney test. n.s., not significant

antibody (Invitrogen) in Perm/Wash Buffer for 30 min on ice. The cells were then washed and analyzed using flow cytometry.

Statistical analysis

Data were analyzed using GraphPad Prism version 9 or 10.

Results

IL-7R$^{\Delta Treg}$ mice have fewer VAT Tregs and show impaired glucose tolerance

To examine the function of IL-7Rα in tissue Tregs, *Foxp3*$^{YFP\text{-}Cre}$ mice were crossed with *IL-7Rα*–floxed mice.[26,27] The resulting *Foxp3*$^{YFP\text{-}Cre}$ *IL7rα*$^{flox/flox}$ (IL-7R$^{\Delta Treg}$) mice appeared healthy, showed no visible autoimmune symptoms, and maintained a body weight comparable to that of control *Foxp3*$^{YFP\text{-}Cre}$*IL7rα*$^{+/+}$ mice under specific pathogen–free conditions (Fig. S1A). Successful IL-7Rα deletion was limited to Foxp3$^+$ CD4 T cells (Fig. S1B). The frequency and number of Tregs, as well as the ratio of CD44^{low}CCR7^{high} naive Tregs and CD44^{high}CCR7^{low} effector Tregs (eTregs), were similar between control and IL-7R$^{\Delta Treg}$ mice in the spleen and lymph nodes (LNs) (Fig. S1C, D). The ratio of eTregs was slightly reduced in the thymus (Fig. S1D). We then investigated the abdominal VAT, a nonlymphoid tissue where Tregs are more prevalent than in other organs.[11] VAT weights were similar between control and IL-7R$^{\Delta Treg}$ mice (Fig. S1E). However, male and female IL-7R$^{\Delta Treg}$ mice exhibited significantly lower frequencies and numbers of VAT Tregs (Fig. 1A; Fig. S1F). ST2 expression distinguishes tissue Tregs, and ST2$^+$ Tregs are abundant in VAT and produce large amounts of IL-10.[36] In IL-7R$^{\Delta Treg}$ mice, the number of ST2$^+$, but not ST2$^-$, Tregs were reduced by approximately 75% (Fig. 1A, B; Fig. S1G). Consistent with fewer ST2$^+$ Tregs, the frequency of IL-10-producing Tregs decreased in the VAT of IL-7R$^{\Delta Treg}$ mice, and the frequency of IL-10$^+$ ST2$^+$ Tregs appeared to be slightly lower in IL-7R$^{\Delta Treg}$ mice (Fig. 1C). These results indicate that the IL-7Rα plays an essential role in the accumulation of VAT Tregs.

VAT Tregs suppress obesity-associated inflammation, which in turn limits insulin resistance.[11,12] Consistently, IL-7R$^{\Delta Treg}$ mice fed the standard diet and HFD exhibited impaired glucose tolerance (Fig. 1D; Fig. S1H). Insulin resistance was observed in IL-7R$^{\Delta Treg}$ mice fed the standard diet, although the differences were not statistically significant (Fig. S1I). There was no remarkable difference in the histology of hematoxylin and eosin–stained liver sections or in serum triglyceride and total cholesterol levels between control and IL-7R$^{\Delta Treg}$ mice fed a standard diet at 15 wk of age (Fig. 1E; Fig. S1J). However, as type 2 diabetes (T2D) is associated with hepatic steatosis,[37] IL-7R$^{\Delta Treg}$ mice fed an HFD tended to show an increased frequency of lipid droplet deposition in the liver and higher liver triglyceride content (Fig. 1E, F). Furthermore, since hepatic steatosis causes an elevation of blood LDL cholesterol by reducing LDL receptors in the liver,[38,39] IL-7R$^{\Delta Treg}$ mice fed an HFD tended to have slightly elevated blood LDL cholesterol levels (Fig. 1G). These results indicate that IL-7Rα is essential for VAT homeostasis and glucose metabolism through Tregs.

To understand the underlying function of IL-7Rα signaling in VAT Tregs, we analyzed the expression of peroxisome proliferator-activated receptor γ (PPAR-γ) , a master regulator of VAT Treg differentiation.[12] Residual ST2$^+$ VAT Tregs in IL-7R$^{\Delta Treg}$ mice showed normal PPAR-γ expression (Fig. 1H). Furthermore, VAT Tregs cultured ex vivo with IL-7 or TSLP did not increase the frequency of ST2$^+$ Tregs or upregulate ST2 expression (Fig. 1I, J). These results suggest that IL-7Rα signaling is dispensable for PPAR-γ and ST2 expression in VAT Tregs. Because IL-7R signaling supports T cell survival and proliferation, we examined the expression of the antiapoptotic factor Bcl-2 and proliferation marker Ki-67 in VAT Tregs. While Ki-67^{high} Tregs were increased (Fig. S1K), Bcl-2 expression was attenuated in VAT ST2$^+$ Tregs of IL-7R$^{\Delta Treg}$ mice (Fig. 1K), suggesting that the survival of ST2$^+$ VAT Tregs depends on IL-7Rα signaling.

ST2$^+$ Tregs are IL-7Rα^{high}, but their IL-7Rα signaling dependence varies between tissues

To analyze the specific role of IL-7Rα in ST2$^+$ Tregs, we examined IL-7Rα expression levels in Tregs. IL-7Rα expression levels generally discriminate between IL-7R^{high} conventional T cells and IL-7R^{low} Tregs.[20,21] However, VAT Tregs expressed IL-7Rα at high levels, comparable to those of conventional CD4 T cells (Fig. 2A). In the VAT, 80% to 90% of Tregs are ST2-expressing eTregs.[36] Compared with ST2$^-$ Tregs, IL-7Rα expression was higher in ST2$^+$ Tregs in the VAT (Fig. 2A). Because eTregs show higher IL-7Rα expression than naive Tregs and ST2$^+$ Tregs are included in eTregs,[36,40] we compared IL-7Rα expression between naive, ST2$^-$ effector, and ST2$^+$ effector Tregs to investigate whether IL-7R^{high} is a common feature of eTregs or a characteristic of ST2$^+$ eTregs. In the VAT, but also in the spleen, colon, lung, and bone marrow (BM), IL-7Rα expression levels were consistently high in ST2$^+$ eTregs but not in ST2$^-$ eTregs (Fig. 2B), indicating that IL-7Rα^{high} is characteristic of ST2$^+$ eTregs. These results suggest that the IL-7Rα may have a specific function in ST2$^+$ eTregs.

We investigated the effect of IL-7Rα signaling on ST2$^+$ eTregs in different tissues. IL-7R$^{\Delta Treg}$ mice showed no

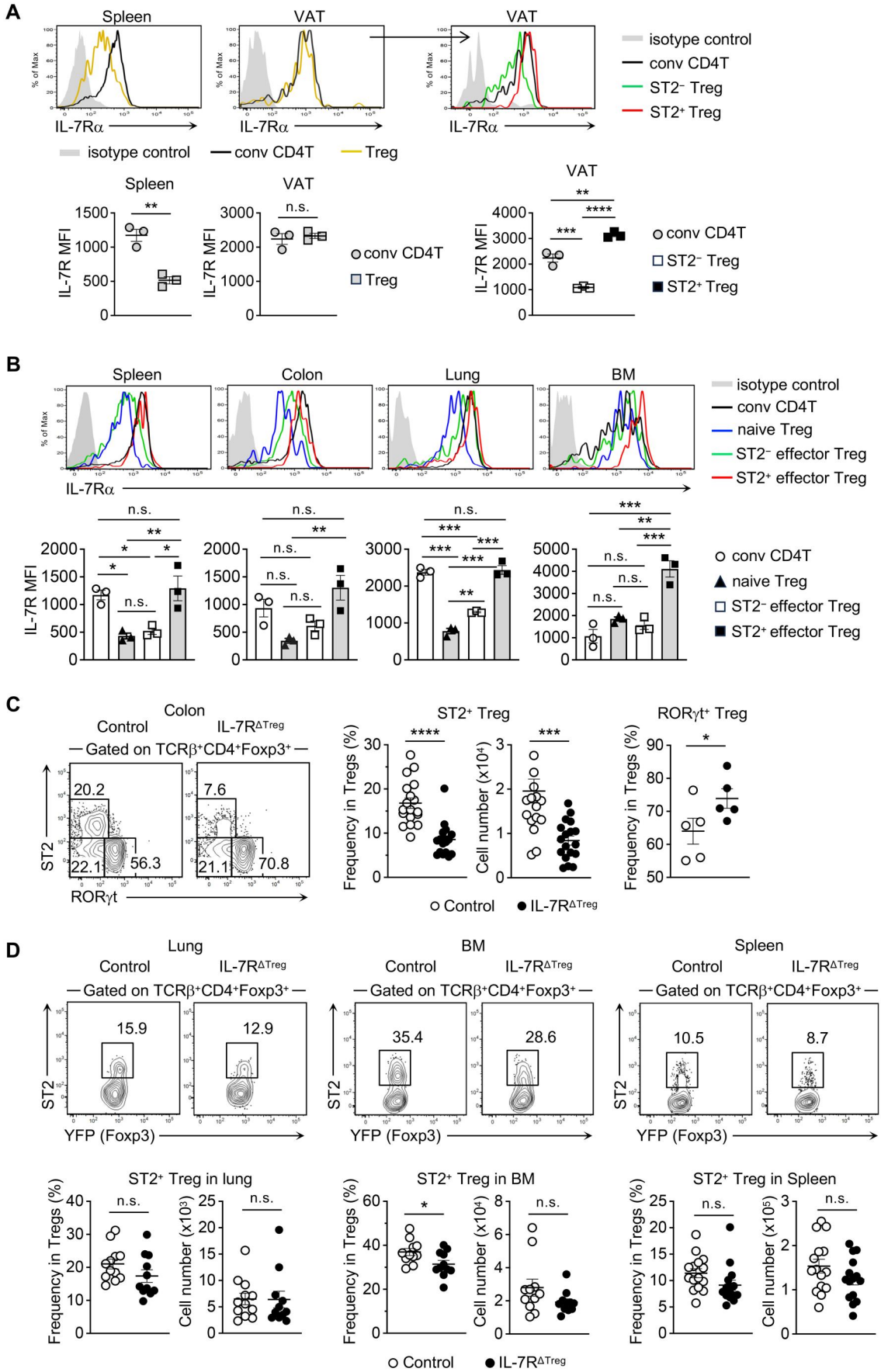

Figure 2. ST2$^+$ Tregs express IL-7Rα at high levels, and their IL-7Rα dependence differs between tissues. (A) IL-7Rα expression in conventional CD4 T cells and Tregs in tissues from wild-type (WT) mice (left). IL-7Rα expression in conventional CD4 T cells and ST2$^+$ and ST2$^-$ Tregs in the VAT (right). Graphs summarize the mean fluorescence intensity (MFI) of IL-7Rα. (B) IL-7Rα expression in conventional CD4 T cells, naive Tregs, and ST2$^+$ and ST2$^-$

(Continued)

Figure 2. Continued
effector Tregs in the indicated tissues. Naive and effector Tregs were defined as TCRβ$^+$CD4$^+$YFP$^+$CD44^{low}CCR7^{high} and TCRβ$^+$CD4$^+$YFP$^+$CD44^{high}CCR7^{low}, respectively. Graphs summarize the MFI of IL-7Rα. (C) Colon ST2$^+$ Tregs in the control and IL-7R$^{\Delta Treg}$ mice at 15 wk of age. The graphs show the frequency and number of ST2$^+$ Tregs (n = 18 mice per group) and the frequency of RORγt$^+$ Tregs (n = 5 mice per group) in the colon. (D) ST2$^+$ Tregs in the indicated tissues of control and IL-7R$^{\Delta Treg}$ mice at 10 to 15 wk of age. The graphs show the frequency and number of ST2$^+$ Tregs. (Lung, n = 11–12 mice per group; BM, n = 11 mice per group; spleen, n = 15 mice per group). (A, B) Wild-type mice were analyzed at 15 wk of age. Shown represents 3 independent flow cytometric analyses. (C, D) The numbers in each plot indicate the percentage of gated populations. (A–D) Data are mean ± SEM. Statistics were performed using unpaired *t* test (A [left], C, D) or 1-way analysis of variance (A [right], B). *$P < 0.05$, **$P < 0.01$, ***$P < 0.001$, ****$P < 0.0001$. conv, conventional; n.s., not significant.

changes in the frequency and number of total Tregs in the colon, lungs, and BM (Fig. S2A). Nevertheless, IL-7R$^{\Delta Treg}$ mice exhibited a 60% reduction in the frequency and number of ST2$^+$ Tregs in the colon (Fig. 2C). Instead, the frequency of RORγt$^+$ Tregs increased in the colon of IL-7R$^{\Delta Treg}$ mice. ST2$^+$ Tregs produce Areg, a growth hormone with tissue-repair activity.[6,7] To investigate the impact of lowered colonic ST2$^+$ Tregs in IL-7R$^{\Delta Treg}$ mice on inflammation and tissue repair, we used a DSS-induced colitis model. Despite the reduced colonic ST2$^+$ Tregs, IL-7R$^{\Delta Treg}$ mice showed comparable body weight loss, disease activity index, and histology, suggesting that IL-7R$^{\Delta Treg}$ mice exhibited unchanged tissue repair during intestinal inflammation (Fig. S2B–D). Many Tregs in the lungs, BM, and spleen express ST2.[5,6] In these organs, the frequency of ST2$^+$ Tregs was unchanged or decreased by 15% in IL-7R$^{\Delta Treg}$ mice (Fig. 2D). These results suggest that, despite the elevated expression of IL-7Rα among ST2$^+$ Tregs, their dependence on IL-7Rα signaling varies among tissues.

Precursor stages of ST2$^+$ tissue Tregs are independent of IL-7Rα

Precursors of ST2$^+$ tissue Tregs have been identified in the secondary lymphoid organs. ST2$^+$ tissue Treg precursors can be divided into 3 stages: Klrg1$^-$*Nfil3*$^-$, Klrg1$^-$*Nfil3*$^+$, and Klrg1$^+$*Nfil3*$^+$ (hereafter referred to as stages 1, 2, and 3, respectively), and differentiate in this order.[5] To examine whether IL-7Rα is required for the development of ST2$^+$ Treg precursors, we analyzed spleens 10 d after birth, when the frequency of precursors peaks.[5] Using KLRG1 and E4BP4 (encoded by *Nfil3*) antibodies, we found that the frequency and number of ST2$^+$ Treg precursors were unaffected in the spleen of IL-7R$^{\Delta Treg}$ mice (Fig. 3A, B). ST2 expression has been reported to begin at stage 3.[5] As IL-7Rα was highly expressed in ST2$^+$ Tregs (Fig. 2B), IL-7Rα expression was low in stages 1 and 2 and was upregulated in stage 3 at the RNA level (Fig. 3C). Pd1 can be substituted by *Nfil3*.[5] Similarly, Pd1 distinguished between Treg precursor stages in control and IL-7R$^{\Delta Treg}$ mice (Fig. 3D). Consistent with RNA expression, IL-7Rα surface expression was low in stages 1 and 2 and high in stage 3 (Fig. 3E). Although the frequency of ST2$^+$ Tregs was slightly reduced at stage 3 in IL-7R$^{\Delta Treg}$ mice (Fig. 3F), these numbers were not significantly reduced (Fig. 3G). Collectively, IL-7Rα signaling does not affect the differentiation of ST2$^+$ Treg cells at stage 1 and 2 precursor stages in secondary lymphoid organs.

TSLP is partially responsible for adipose ST2$^+$ Tregs

Possible ligands of IL-7Rα include IL-7 and TSLP. We analyzed the expression of the TSLPR to determine whether TSLP is required for ST2$^+$ VAT Tregs. TSLPR was highly expressed in VAT Tregs, especially in ST2$^+$ eTregs (Fig. 4A), which is consistent with a recent report that TSLPR$^+$ Tregs in colorectal cancer express ST2.[41] TSLPR was also highly expressed in ST2$^+$ eTregs in various tissues, similar to IL-7Rα (Fig. S3A). To investigate the effects of TSLP on VAT Tregs, we generated TSLP-deficient (TSLP KO) mice (Fig. S3B–E). As seen in IL-7R$^{\Delta Treg}$ mice, the frequency, number, and naive/effector ratio of Tregs in the spleen of TSLP KO mice remained unchanged (Fig. S3F, G). However, TSLP KO mice showed a slight decrease in frequency and a trend toward a reduced number of VAT Foxp3$^+$ cells (Fig. 4B). Although the frequency and number of VAT ST2$^+$ Tregs were reduced by approximately 30% in TSLP KO mice (Fig. 4C), the reduction was less severe than that in IL-7R$^{\Delta Treg}$ mice. TSLP KO mice also exhibited slightly impaired glucose tolerance (Fig. 4D), which was less severe than that in IL-7R$^{\Delta Treg}$ mice, as the area under the curve of the glucose tolerance test remained unchanged in TSLP KO mice (Fig. 4E). We further analyzed ST2$^+$ Tregs in other tissues of TSLP KO mice. In contrast to IL-7R$^{\Delta Treg}$ mice, the number of Tregs, including ST2$^+$ populations, did not change in the colon of TSLP KO mice (Fig. 4F; Fig. S3H), suggesting that IL-7, rather than TSLP, may support ST2$^+$ Tregs in the colon. However, in the lung and BM, TSLP KO mice exhibited a 30% reduction in the frequency and number of ST2$^+$ Tregs while the total number of Treg cells remained unchanged (Fig. 4F; Fig. S3H), suggesting that TSLP partially supports ST2$^+$ Tregs in these tissues. Collectively, these results suggest that TSLP cooperates with IL-7 to maintain VAT ST2$^+$ Tregs.

TSLP is required for glucose homeostasis via eosinophil accumulation in adipose tissue

Despite the slight decrease in VAT Tregs (Fig. 4B), TSLP KO mice exhibited impaired glucose tolerance, even when fed a standard diet (Fig. 4D). To further explore the reasons for glucose intolerance in TSLP KO mice, we investigated the VAT. Although conventional CD4 and CD8 T cells are reportedly involved in sebum-induced white adipose loss through TSLP,[18] VAT weight and conventional T cell numbers remained unchanged in TSLP KO mice (Fig. 5A; Fig. S4A, B). Because adipose tissue eosinophils play a crucial role in maintaining glucose homeostasis by suppressing inflammation through IL-4–mediated M2 macrophage polarization,[13] we examined the impact of TSLP deletion on VAT eosinophils (Fig. S4C). As previously reported for TSLPR-deficient mice,[42] the number of lung eosinophils remained unchanged in TSLP KO mice (Fig. S4D), whereas VAT eosinophils were reduced by 50% in TSLP KO mice (Fig. 5B; Fig. S4E).

Because IL-5 produced by ILC2s is critical for eosinophil accumulation in the VAT,[14] we next examined ILC2s. The number of VAT ILC2s in TSLP KO mice was unaffected (Fig. 5C; Fig. S4F), consistent with a previous report that the number of lung ILC2s is unchanged at steady state in TSLPR KO mice.[43] In the lung, loss of TSLPR does not affect IL-5 production by ILC2s at steady state,[44] although stimulation with TSLP and IL-33 increases IL-5 production ex vivo.[45] To

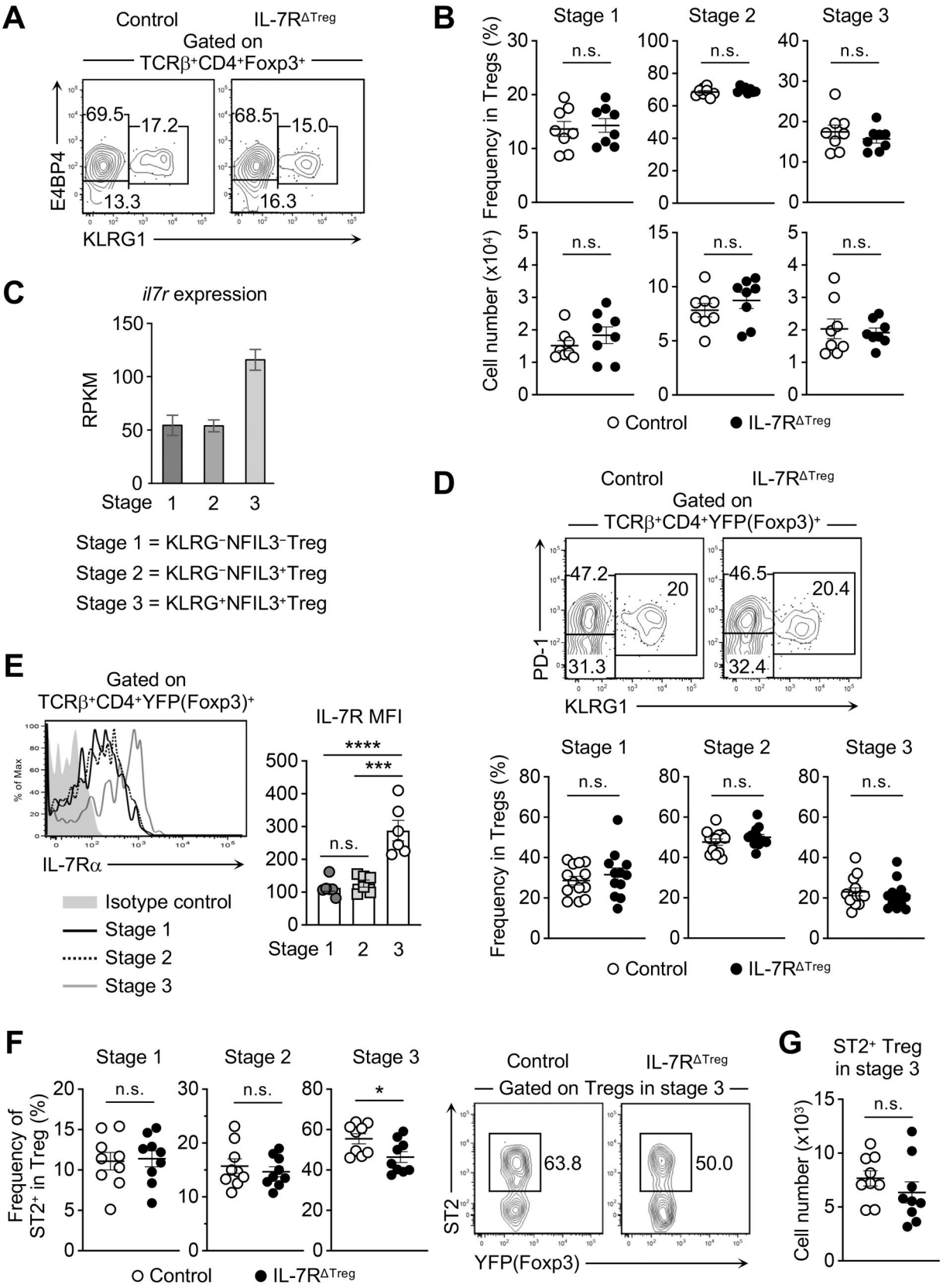

Figure 3. ST2$^+$ tissue Treg precursors do not require IL-7Rα. (A) E4BP4 and KLRG1 expression in TCRβ$^+$CD4$^+$Foxp3$^+$ cells in the spleen of control and IL-7R$^{\Delta Treg}$ mice at day 10 after birth. Shown represents 8 mice from 4 independent experiments. (B) Frequency and number of stage 1 (E4BP4$^-$KLRG1$^-$), stage 2 (E4BP4$^+$KLRG1$^-$), and stage 3 (E4BP4$^+$KLRG1$^+$) tissue Treg precursors in the spleen on day 10 after birth (n = 8 mice per group). (C) The bar graph indicates the RPKM of *Il7r* obtained from GSE130842. (D) PD-1 and KLRG1 expression in TCRβ$^+$CD4$^+$YFP(Foxp3)$^+$ cells in the spleen of control and IL-7R$^{\Delta Treg}$ mice at day 10 after birth. Shown represents more than 10 mice. The graphs show the frequency of stage 1 (PD-1$^-$KLRG1$^-$), stage 2 (PD-1$^+$KLRG1$^-$), and stage 3 (PD-1$^+$KLRG1$^+$) in Tregs. (E) Flow cytometric analysis of IL-7Rα expression in the spleen of postnatal day 10 Foxp3$^{YFP\text{-}Cre}$ mice in stage 1, 2, and 3 tissue Treg precursors separated by PD-1 and KLRG-1. Shown represents 6 mice from 3 independent experiments. The graph

(Continued)

Figure 3. Continued
summarizes the mean fluorescence intensity (MFI) of IL-7Rα. (F) Frequency of ST2$^+$ populations at stages 1, 2, and 3 tissue Treg precursors in control and IL-7R$^{\Delta Treg}$ mice on day 10 after birth (n = 9 mice per group). Plots represent ST2 expression at stage 3. (G) Number of ST2$^+$ cells in stage 3 tissue Treg precursors (n = 9 mice per group). (A–G) The numbers in each plot indicate the percentage of gated populations. Data are mean ± SEM. Statistics were performed using unpaired *t* test (B, D, F, G) or 1-way analysis of variance (E). *$P < 0.05$, ***$P < 0.001$, ****$P < 0.0001$. n.s., not significant.

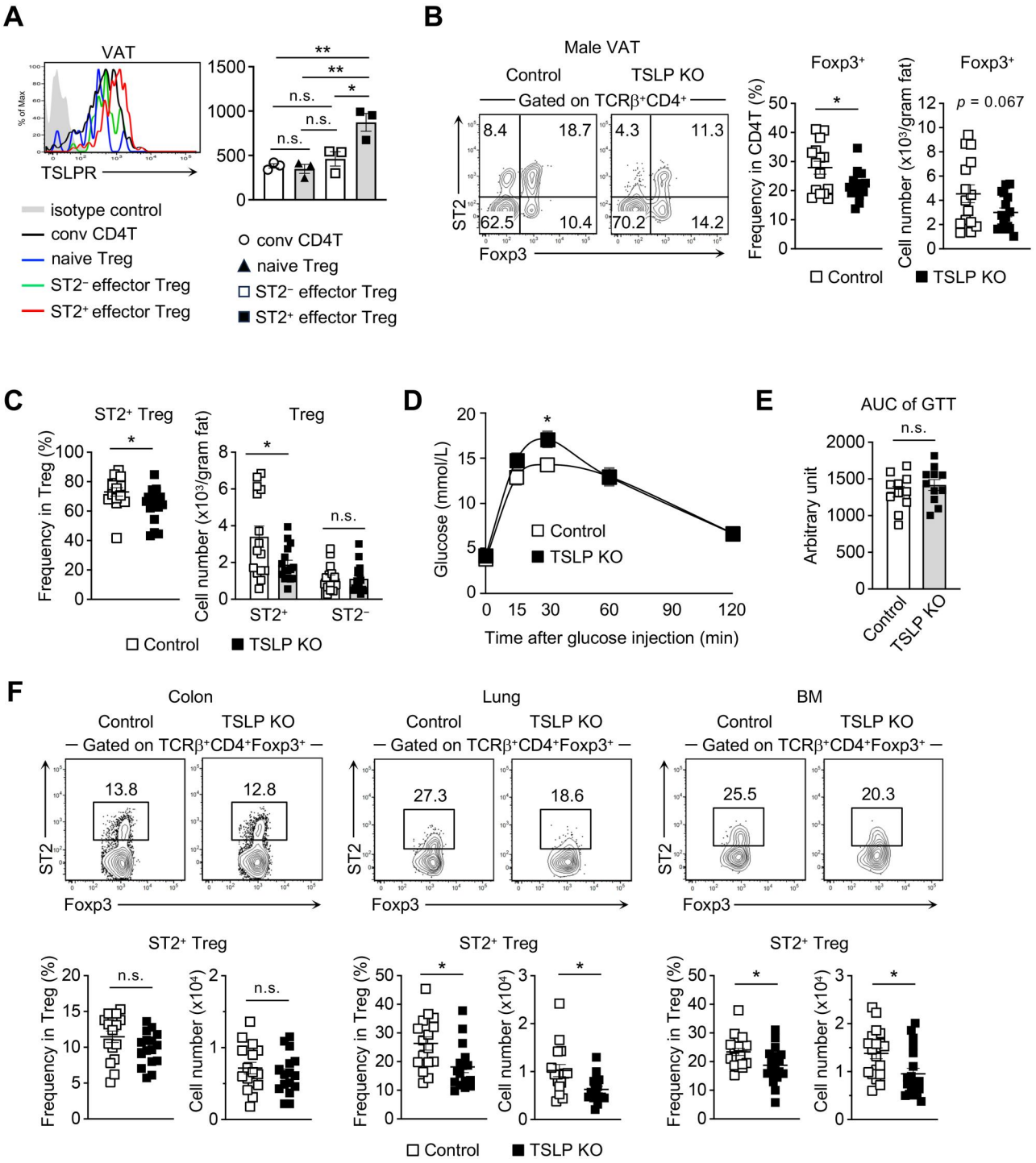

Figure 4. (A) TSLP is partially responsible for VAT Treg TSLPR expression in VAT Tregs of WT mice. Data represent 3 independent experiments. The graph summarizes the MFI of TSLPR. (B) Tregs in the VAT of control and TSLP KO male mice fed a standard diet at 15 wk of age. The graphs show the frequency of Tregs among VAT CD4 T cells and the number of VAT Tregs (n = 15–16 mice per group). (C) Frequency of ST2$^+$ Tregs among VAT Tregs and the number of ST2$^+$ and ST2$^-$ VAT Tregs in 15-wk-old control and TSLP KO male mice (n = 15–16 mice per group). (D) GTT was performed on control and TSLP KO mice fed a standard diet at 15 wk of age (n = 11 mice per group). (E) The area under the curve (AUC) of GTT in Fig. 3D was calculated using GraphPad Prism. (F) ST2$^+$ Tregs in the indicated tissues of control and TSLP KO male mice fed with a standard diet at 15 wk of age. The graphs show the frequency and number of ST2$^+$ Tregs in indicated tissues (n > 15 mice per group). (B, F) The numbers in each plot indicate the percentage of gated populations. (A–F) Data are mean ± SEM. Statistics were performed using 1-way analysis of variance (A) and unpaired *t* test (B–F). *$P < 0.05$, **$P < 0.01$. conv, conventional; n.s., not significant.

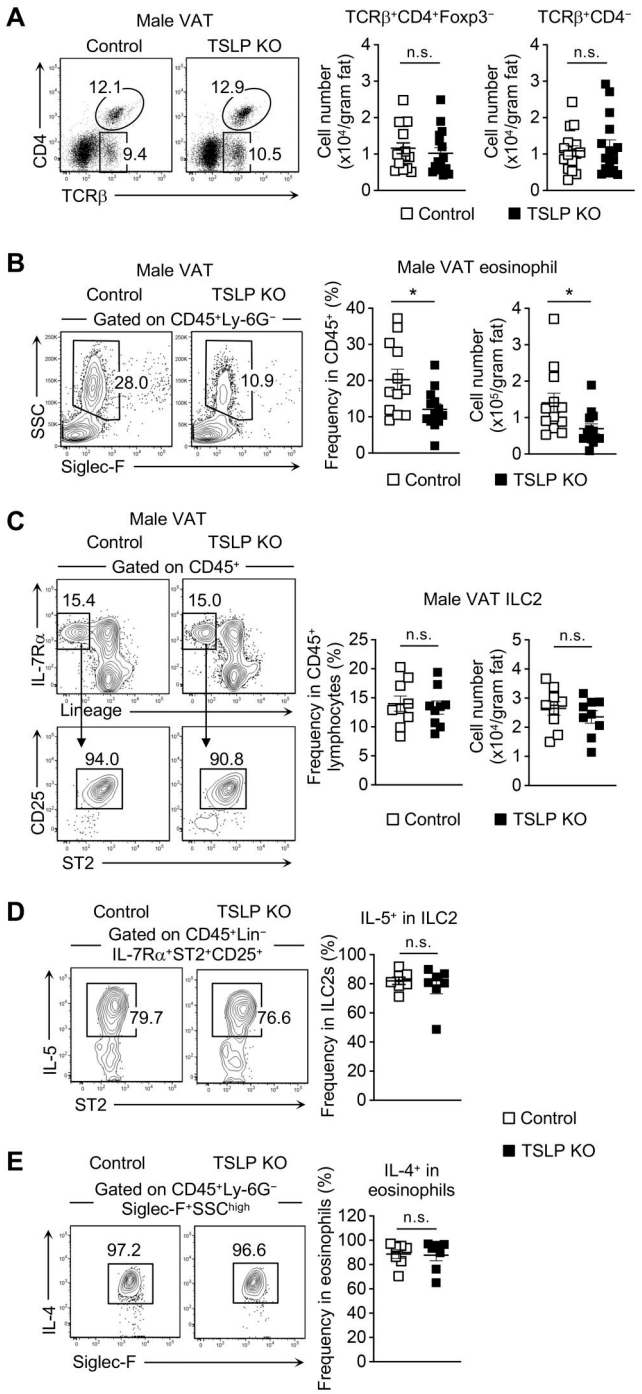

Figure 5. Adipose eosinophils are reduced at steady state in TSLP-deficient mice. (A) Conventional T cells in VAT of control and TSLP KO mice. The graphs show the number of VAT CD4 (Foxp3^{-}CD4^{+}TCRβ^{+}) and CD8 (CD4^{-}TCRβ^{+}) T cells (n = 16 mice per group). (B) VAT eosinophils (CD45^{+}Ly-6G^{-}Siglec-F^{+}SSC^{high}) in control and TSLP KO mice. The graphs show the frequency (Ly-6G^{-}Siglec-F^{+}SSC^{high} in CD45^{+}) and number of VAT eosinophils in the indicated mice (n = 12–13 mice per group). (C) VAT ILC2s (CD45^{+}Lin^{-}IL-7Rα^{+}CD25^{+}ST2^{+}) in control and TSLP KO mice. The graphs show the frequency (Lin^{-}IL-7Rα^{+}CD25^{+}ST2^{+} in CD45^{+}) and number of VAT ILC2s in the indicated mice (n = 9 mice per group). (D) IL-5 production by VAT ILC2s. VAT SVF cells were stimulated with PMA and ionomycin for 4 h. Frequency of IL-5^{+} ILC2s was determined by gating on ILC2s as in panel C (n = 7 mice per group). (E) IL-4 production by VAT eosinophils. VAT SVF cells were stimulated with PMA and ionomycin for 4 h. Frequency of IL-4^{+} eosinophils was determined by gating on eosinophils (CD45^{+}Gr-1^{-}Siglec-F^{+}CD11b^{+}CD11c^{int}) (n = 7 mice per group). (A–E) Male mice fed a

(Continued)

Figure 5. Continued
standard diet at 12 to 15 wk of age were used. Numbers in each plot indicate the percentage of gated populations. Data are mean ± SEM. Statistics were performed using unpaired *t* test. $^{*}P < 0.05$. n.s., not significant.

investigate the impact of TSLP deficiency on IL-5 production by adipose ILC2s, we cultured the SVF cells of the VAT with PMA and ionomycin and performed intracellular staining. IL-5 production by VAT ILC2s was unaffected in TSLP KO mice (Fig. 5D). Furthermore, TSLP deficiency did not affect the ability of eosinophils to produce IL-4 ex vivo (Fig. 5E). Because eosinophils did not express IL-7Rα but expressed TSLPR at low levels (Fig. S4G), the effect of TSLP on eosinophil accumulation in VAT remains unclear. Nevertheless, our data suggest that TSLP facilitates VAT eosinophil accumulation and thus influences systemic glucose homeostasis.

Source of IL-7 and TSLP in the VAT

Our findings that IL-7Rα expression on Tregs and TSLP-mediated eosinophil accumulation regulate systemic glucose homeostasis raise a novel role for IL-7 and TSLP in adipose tissue. However, IL-7– and TSLP-producing cells in VAT have not been identified. To this end, we reanalyzed the scRNA-seq data of stromal and hematopoietic cells in epididymal white adipose tissue (Fig. 6A).[33] IL-7 was mainly detected in *Msln* (mesothelin)-, *Wt1*-, and *Cd9*-expressing mesothelial cells (Fig. 6B).[46] We further analyzed IL-7 expression in VAT stromal cells using IL-7^{GFP} knock-in mice. We used flow cytometry because immunofluorescence staining could not detect GFP signals in VAT (not shown). We found that PDGFRα^{-} gp38^{+} (encoded by *Pdpn*) stromal cells expressed IL-7 (Fig. 6C). This population is consistent with previously reported IL-33 producers in VAT.[47] Consistently, *Il33*$^{+}$ cells were detected in the same cluster that expressed *Il7* (Fig. 6D). In contrast, *Tslp*-expressing cells were detected in adipose stem cells (ASCs) (Fig. 6E). Two main populations, ASC1s and ASC2s, can be distinguished, and *Col115a1* and *Sbsn* expression is enriched in ASC1s and ASC2s, respectively.[33,46] *Tslp*$^{+}$ cells were distributed in both ASC1s and ASC2s (Fig. 6E). *Tslp* was also detected in *Adgre1* (F4/80)- and *Mafb*-expressing macrophages (Fig. 6E). These cells expressed high levels of *Folr2* (encoding folate receptor β), a marker of tissue-resident macrophages (Fig. 6E).[48] Collectively, these data suggest that adipose mesothelial cells produce IL-7 in the VAT, whereas ASCs and adipose tissue-resident macrophages mainly produce TSLP.

Discussion

In terms of development, the number of Tregs is reduced in IL-7Rα–deficient mice, although the ratio of Tregs to conventional CD4 T cells remains unaffected.[49–51] In addition, Tregs are maintained less in IL-7$^{-/-}$Rag$^{-/-}$ mice than in Rag$^{-/-}$ mice,[52] and memory Tregs in the skin are diminished by IL-7Rα–blocking antibody.[53] IL-7 has been proposed to be necessary for the survival of Tregs in LNs, based on a study employing IL-7 transgenic mice.[54] In contrast, Tregs in skin-draining LNs from *Foxp3*$^{YFP\text{-}Cre}$ *IL7rα*$^{flox/flox}$ mice are comparable to those in control mice.[25] Mature Tregs with a CD25 deletion can survive for several weeks by replacing IL-2 with IL-7. Nevertheless, it has been proposed that Treg survival in the presence of IL-2 does not rely on either IL-7 or IL-15.[24] Here, we confirmed that the

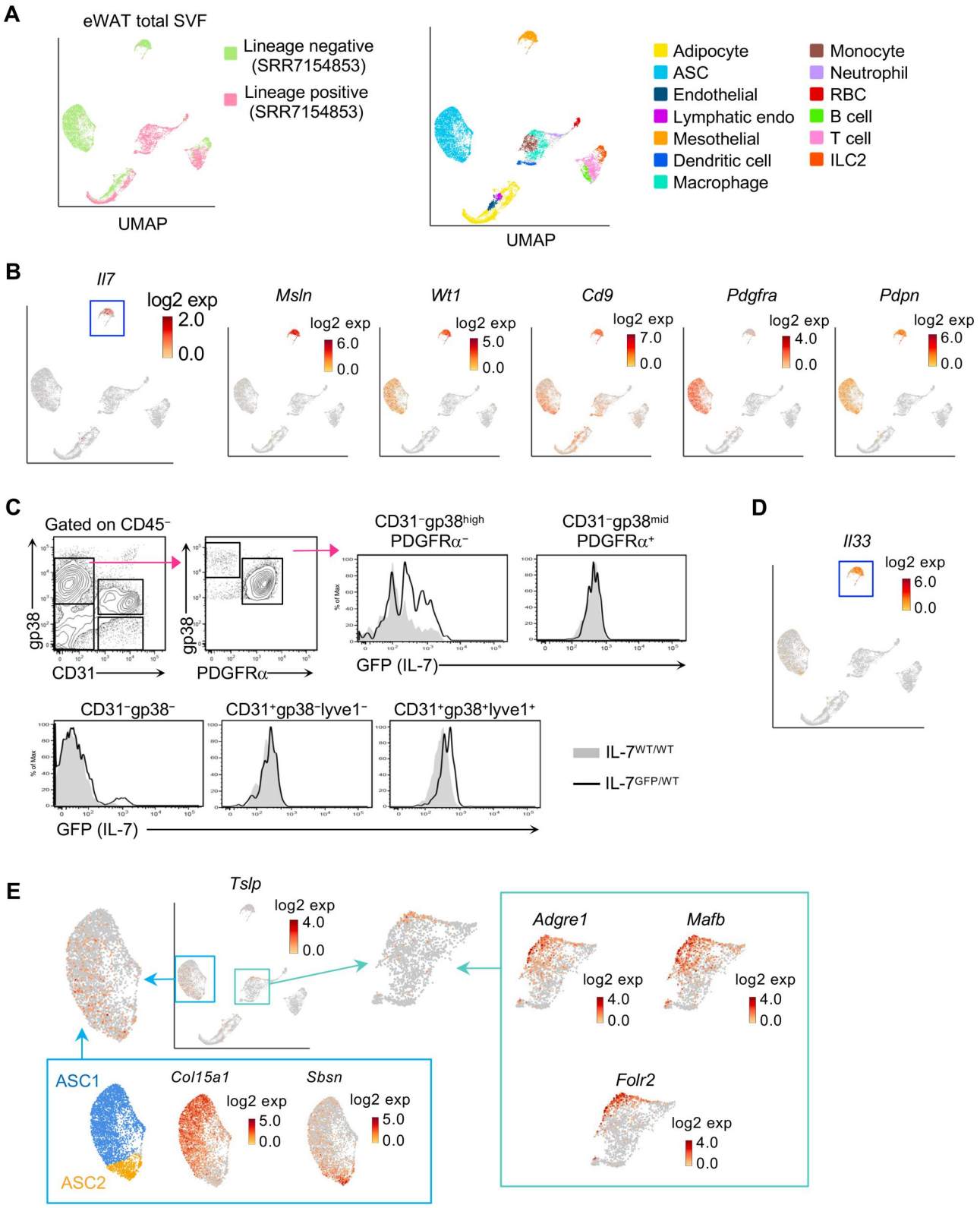

Figure 6. Source of IL-7 and TSLP in adipose tissue. (A) Uniform Manifold Approximation and Projection (UMAP) of scRNA-seq data from epididymal white adipose tissue (eWAT) hematopoietic lineage–negative (SRR7154853) and –positive (SRR7154855) SVF cells. The cell identity of each cluster was defined based on the marker gene expression (see Materials and Methods). (B) UMAP plots showing log2 expression levels of *Il7* and the selected genes. (C) CD45⁻ stromal cells in the SVF of the VAT from *IL7*$^{WT/WT}$ and *IL7*$^{GFP/WT}$ mice. Intracellular IL-7 (GFP) staining was performed. Shown represents 5 independent experiments. (D) UMAP plots showing log2 expression levels of *Il33*. (E) UMAP plots showing log2 expression levels of *Tslp* and the selected genes. RBC, red blood cell.

absence of IL-7Rα has no impact on the development, maintenance, and naive/effector ratio of Tregs in thymus and secondary lymphoid tissues.

While low IL-7R expression is frequently considered a characteristic of Tregs, it is not consistently observed across all tissues. In particular, Tregs in the bone marrow and skin exhibit high levels of IL-7Rα.[40] Our study revealed the essential role of highly expressed IL-7Rα in maintaining $ST2^+$ effector Tregs in the VAT and colon. Furthermore, $ST2^+$ Tregs display elevated Areg levels, which are critical for tissue repair.[6,7] However, there was no notable difference in the severity of DSS-induced colitis in IL-$7R^{\Delta Treg}$ mice despite the reduced number of $ST2^+$ Tregs. In IL-33–deficient mice with fewer $ST2^+$ Tregs, an increase in $ST2^-$RORγt^+ Tregs was observed instead.[55] Similarly, RORγt^+ Tregs increased in IL-$7R^{\Delta Treg}$ mice, which may have resulted in reduced inflammation.

Anti-IL-7Rα antibodies are expected to provide a novel therapeutic approach for the treatment of type 1 diabetes (T1D).[56,57] In NOD mice, administration of antagonistic anti-IL-7Rα antibodies successfully induces complete remission of T1D.[58,59] A phase Ib study has reported on IL-7R blockade.[60] Administration of RN168, a humanized monoclonal antibody blocking human IL-7RA, decreased peripheral blood memory and effector T cells but maintaind Tregs. However, our findings suggest that IL-7R signaling can affect $ST2^+$ Tregs in adipose tissue. Therefore, blocking IL-7Rα may benefit T1D but could also increase the risk of developing T2D.

It has been suggested that TSLP impairs the suppressive activity and IL-10 production of human pulmonary Tregs.[61] Nevertheless, our study indicates that TSLP partially supports the maintenance of $ST2^+$ Tregs and eosinophils in the VAT, leading to glucose homeostasis. Notably, human peripheral blood eosinophils express both IL-7Rα and TSLPR,[62,63] and TSLP treatment promotes the survival and activation of human eosinophils, leading to eosinophil extracellular trap formation and degranulation.[62–64] In contrast, murine eosinophils did not express IL-7Rα. The mechanism underlying the reduction in VAT eosinophils in TSLP KO mice remains unknown. Other receptors may mediate TSLP signaling in eosinophils besides the TSLPR/IL-7Rα heterodimer. Another possibility is that TSLP may indirectly influence eosinophil accumulation. For example, TSLP may promote the production of granulocyte-macrophage colony-stimulating factor by ILC2s, leading to eosinophil accumulation.[65] TSLP may indirectly help VAT Tregs and eosinophils to survive and proliferate. There are no reports on these populations in the VAT of Treg- or eosinophil-specific TSLPR-deficient mice. $CD4^+$ and $CD8^+$ T cells reportedly mediate TSLP-induced adipose tissue loss.[18] Loss of TSLP may cause changes in the adipose tissue environment, resulting in a partial loss of Tregs and eosinophils.

IL-33 plays a critical role in the accumulation of Tregs and the activation of ILC2s in the VAT.[36,66] Despite being a minor population in the VAT, mesothelial cells produce IL-33 at high levels. Mesothelial cells form a cobblestone monolayer on the visceral and parietal surfaces of the peritoneal, pleural, and pericardial cavities.[67] Interestingly, mesothelial cells are not present in subcutaneous adipose tissue, and Tregs are less abundant in subcutaneous adipose tissue than in VAT.[11,67] This study highlights the importance of mesothelial cells as a crucial source of IL-7 in VAT, enabling the creation of an ideal environment for Tregs. Moreover, scRNA-seq analysis identified tissue-resident macrophages expressing TSLP and folate receptor β. Recent studies have revealed that tissue-resident macrophages can produce TSLP in the skin and lung.[68,69] Our study suggests that adipose tissue-resident macrophages function in TSLP production, leading to eosinophil accumulation.

The unexpected role of IL-7Rα signaling in VAT $ST2^+$ Tregs indicates that IL-7 produced by VAT mesothelial cells plays a crucial role in regulating glucose homeostasis. Additionally, TSLP is essential for proper eosinophil accumulation in the adipose tissue. These findings suggest that IL-7 and TSLP may be potential therapeutic targets for T2D.

Acknowledgments

The authors thank Dr. A. Rudensky (Memorial Sloan Kettering Cancer Center) for providing $Foxp3^{YFP\text{-}Cre}$ mice and members of the Ikuta laboratory for discussions.

Author contributions

S.T. designed and performed the experiments. S.A. helped with RNA-seq analysis. H.M. and S.K. helped to generate TSLP KO mice. T.K. and K.T. helped insulin tolerance test experiment. A.E., A.S., T.H., and G.C. helped with some experiments. S.H. provided reagents. S.T. and K.I. wrote the paper.

Supplementary material

Supplementary material is available at *The Journal of Immunology* online.

Funding

This study was supported by JSPS KAKENHI (grant numbers 19K08999 and 23K06595 to S.T. and grant numbers 20H03501 and 23K27426 to K.I.) and the Shimizu Foundation for Immunology and Neuroscience Grant for 2018 to S.T..

Conflicts of interest

The authors have no conflicts of interest to declare.

Data availability

The data underlying this article are available from the corresponding author on reasonable request.

References

1. Zhou X, Tang J, Cao H, Fan H, Li B. Tissue resident regulatory T cells: novel therapeutic targets for human disease. Cell Mol Immunol. 2015;12:543–552.
2. Campbell C, Rudensky A. Roles of regulatory T cells in tissue pathophysiology and metabolism. Cell Metab. 2020;31:18–25.
3. Delacher M et al. Genome-wide DNA-methylation landscape defines specialization of regulatory T cells in tissues. Nat Immunol. 2017;18:1160–1172.
4. DiSpirito JR et al. Molecular diversification of regulatory T cells in nonlymphoid tissues. Sci Immunol. 2018;3:eaat5861.

5. Delacher M et al. Precursors for nonlymphoid-tissue Treg cells reside in secondary lymphoid organs and are programmed by the transcription factor BATF. Immunity. 2020;52:295–312.e11.
6. Schiering C et al. The alarmin IL-33 promotes regulatory T-cell function in the intestine. Nature. 2014;513:564–568.
7. Arpaia N et al. A distinct function of regulatory T cells in tissue protection. Cell. 2015;162:1078–1089.
8. Munoz-Rojas AR, Mathis D. Tissue regulatory T cells: regulatory chameleons. Nat Rev Immunol 2021;21:597–611.
9. Uysal KT, Wiesbrock SM, Marino MW, Hotamisligil GS. Protection from obesity-induced insulin resistance in mice lacking TNF-α function. Nature. 1997;389:610–614.
10. McNelis JC, Olefsky JM. Macrophages, immunity, and metabolic disease. Immunity. 2014;41:36–48.
11. Feuerer M et al. Lean, but not obese, fat is enriched for a unique population of regulatory T cells that affect metabolic parameters. Nat Med. 2009;15:930–939.
12. Cipolletta D et al. PPAR-γ is a major driver of the accumulation and phenotype of adipose tissue Treg cells. Nature. 2012; 486:549–553.
13. Wu D et al. Eosinophils sustain adipose alternatively activated macrophages associated with glucose homeostasis. Science. 2011; 332:243–247.
14. Molofsky AB et al. Innate lymphoid type 2 cells sustain visceral adipose tissue eosinophils and alternatively activated macrophages. J Exp Med. 2013;210:535–549.
15. Pandey A et al. Cloning of a receptor subunit required for signaling by thymic stromal lymphopoietin. Nat Immunol. 2000;1:59–64.
16. Ebina-Shibuya R, Leonard WJ. Role of thymic stromal lymphopoietin in allergy and beyond. Nat Rev Immunol. 2023;23:24–37.
17. Al-Shami A et al. A role for thymic stromal lymphopoietin in $CD4^+$ T cell development. J Exp Med. 2004;200:159–168.
18. Choa R et al. Thymic stromal lymphopoietin induces adipose loss through sebum hypersecretion. Science. 2021;373:eabd2893.
19. Kashiwagi M et al. Direct control of regulatory T cells by keratinocytes. Nat Immunol. 2017;18:334–343.
20. Liu W et al. CD127 expression inversely correlates with FoxP3 and suppressive function of human $CD4^+$ T reg cells. J Exp Med. 2006;203:1701–1711.
21. Seddiki N et al. Expression of interleukin (IL)-2 and IL-7 receptors discriminates between human regulatory and activated T cells. J Exp Med 2006;203:1693–1700.
22. Chinen T et al. An essential role for the IL-2 receptor in Treg cell function. Nat Immunol. 2016;17:1322–1333.
23. Fehervari Z, Sakaguchi S. Development and function of $CD25^+CD4^+$ regulatory T cells. Curr Opin Immunol. 2004; 16:203–208.
24. Fan MY et al. Differential roles of IL-2 signaling in developing versus mature Tregs. Cell Rep 2018;25:1204–1213.e4.
25. Schmaler M et al. IL-7R signaling in regulatory T cells maintains peripheral and allograft tolerance in mice. Proc Natl Acad Sci U S A. 2015;112:13330–13335.
26. Tani-ichi S et al. Interleukin-7 receptor controls development and maturation of late stages of thymocyte subpopulations. Proc Natl Acad Sci U S A. 2013;110:612–617.
27. Rubtsov YP Jr., et al. Regulatory T cell-derived interleukin-10 limits inflammation at environmental interfaces. Immunity. 2008; 28:546–558.
28. Hara T et al. Identification of IL-7-producing cells in primary and secondary lymphoid organs using IL-7-GFP knock-in mice. J Immunol. 2012;189:1577–1584.
29. Miyao T et al. Plasticity of $Foxp3^+$ T cells reflects promiscuous Foxp3 expression in conventional T cells but not reprogramming of regulatory T cells. Immunity. 2012;36:262–275.
30. Mukohira H et al. Mesenchymal stromal cells in bone marrow express adiponectin and are efficiently targeted by an adiponectin promoter-driven Cre transgene. Int Immunol. 2019;31:729–742.
31. Huynh E, Penney J, Caswell J, Li J. Protective effects of protegrin in dextran sodium sulfate-induced murine colitis. Front Pharmacol. 2019;10:156.
32. Svetic A et al. Cytokine gene expression after in vivo primary immunization with goat antibody to mouse IgD antibody. J Immunol. 1991;147:2391–2397.
33. Burl RB et al. Deconstructing Adipogenesis Induced by β3-adrenergic receptor activation with single-cell expression profiling. Cell Metab. 2018;28:300–309.e4.
34. Emont MP et al. A single-cell atlas of human and mouse white adipose tissue. Nature. 2022;603:926–933.
35. Grupillo M et al. An improved intracellular staining protocol for efficient detection of nuclear proteins in YFP-expressing cells. Biotechniques. 2011;51:417–420.
36. Vasanthakumar A et al. The transcriptional regulators IRF4, BATF and IL-33 orchestrate development and maintenance of adipose tissue-resident regulatory T cells. Nat Immunol. 2015; 16:276–285.
37. Gross B, Pawlak M, Lefebvre P, Staels B. PPARs in obesity-induced T2DM, dyslipidaemia and NAFLD. Nat Rev Endocrinol. 2017;13:36–49.
38. Min HK et al. Increased hepatic synthesis and dysregulation of cholesterol metabolism is associated with the severity of nonalcoholic fatty liver disease. Cell Metab. 2012;15:665–674.
39. Lebeau PF et al. Diet-induced hepatic steatosis abrogates cell-surface LDLR by inducing de novo PCSK9 expression in mice. J Biol Chem. 2019;294:9037–9047.
40. Simonetta F et al. Increased CD127 expression on activated $FOXP3^+CD4^+$ regulatory T cells. Eur J Immunol. 2010; 40:2528–2538.
41. Obata-Ninomiya K, de Jesus Carrion S, Hu A, Ziegler SF. Emerging role for thymic stromal lymphopoietin-responsive regulatory T cells in colorectal cancer progression in humans and mice. Sci Transl Med. 2022;14:eabl6960.
42. Lai JF, Thompson LJ, Ziegler SF. TSLP drives acute T_H2-cell differentiation in lungs. J Allergy Clin Immunol. 2020;146: 1406–1418.e7. e1407.
43. Van Dyken SJ et al. Chitin activates parallel immune modules that direct distinct inflammatory responses via innate lymphoid type 2 and γ δ T cells. Immunity. 2014;40:414–424.
44. Toki S Jr., et al. TSLP and IL-33 reciprocally promote each other's lung protein expression and ILC2 receptor expression to enhance innate type-2 airway inflammation. Allergy. 2020;75:1606–1617.
45. Halim TY, Krauss RH, Sun AC, Takei F. Lung natural helper cells are a critical source of Th2 cell-type cytokines in protease allergen-induced airway inflammation. Immunity. 2012;36:451–463.
46. Rondini EA, Granneman JG. Single cell approaches to address adipose tissue stromal cell heterogeneity. Biochem J. 2020; 477:583–600.
47. Kohlgruber AC et al. γδ T cells producing interleukin-17A regulate adipose regulatory T cell homeostasis and thermogenesis. Nat Immunol 2018;19:464–474.
48. Samaniego R et al. Folate receptor β (FRβ) expression in tissue-resident and tumor-associated macrophages associates with and depends on the expression of PU.1. Cells. 2020;9:1445.
49. Vang KB et al. IL-2, -7, and -15, but not thymic stromal lymphopoeitin, redundantly govern $CD4^+Foxp3^+$ regulatory T cell development. J Immunol. 2008;181:3285–3290.
50. Mazzucchelli R et al. Development of regulatory T cells requires IL-7Rα stimulation by IL-7 or TSLP. Blood. 2008; 112:3283–3292.
51. Bayer AL, Lee JY, de la Barrera A, Surh CD, Malek TR. A function for IL-7R for $CD4^+CD25^+Foxp3^+$ T regulatory cells. J Immunol. 2008;181:225–234.
52. Simonetta F et al. Interleukin-7 influences $FOXP3^+CD4^+$ regulatory T cells peripheral homeostasis. PLoS One. 2012;7:e36596.
53. Gratz IK et al. Memory regulatory T cells require IL-7 and not IL-2 for their maintenance in peripheral tissues. J Immunol. 2013; 190:4483–4487.
54. Kim GY et al. An in vivo IL-7 requirement for peripheral $Foxp3^+$ regulatory T cell homeostasis. J Immunol 2012;188:5859–5866.
55. Hung LY et al. Cellular context of IL-33 expression dictates impact on anti-helminth immunity. Sci Immunol. 2020;5:eabc6259.

56. Harrison C. Autoimmune disease: targeting IL-7 reverses type 1 diabetes. Nat Rev Drug Discov 2012;11:599.
57. Ziegler AG, Bonifacio E. Shortening the paths to type 1 diabetes mellitus prevention. Nat Rev Endocrinol. 2021;17:73–74.
58. Penaranda C et al. IL-7 receptor blockade reverses autoimmune diabetes by promoting inhibition of effector/memory T cells. Proc Natl Acad Sci U S A. 2012;109:12668–12673.
59. Lee LF et al. Anti-IL-7 receptor-α reverses established type 1 diabetes in nonobese diabetic mice by modulating effector T-cell function. Proc Natl Acad Sci U S A. 2012;109:12674–12679.
60. Herold KC et al. and RN168 Working Group Immunomodulatory activity of humanized anti-IL-7R monoclonal antibody RN168 in subjects with type 1 diabetes. JCI Insight. 2019;4:e126054.
61. Nguyen KD, Vanichsarn C, Nadeau KC. TSLP directly impairs pulmonary Treg function: association with aberrant tolerogenic immunity in asthmatic airway. Allergy Asthma Clin Immunol. 2010;6:4.
62. Morshed M, Yousefi S, Stöckle C, Simon H-U, Simon D. Thymic stromal lymphopoietin stimulates the formation of eosinophil extracellular traps. Allergy. 2012;67:1127–1137.
63. Wong CK, Hu S, Cheung PF, Lam CW. Thymic stromal lymphopoietin induces chemotactic and prosurvival effects in eosinophils: implications in allergic inflammation. Am J Respir Cell Mol Biol. 2010;43:305–315.
64. Cook EB, Stahl JL, Schwantes EA, Fox KE, Mathur SK. IL-3 and TNFα increase thymic stromal lymphopoietin receptor (TSLPR) expression on eosinophils and enhance TSLP-stimulated degranulation. Clin Mol Allergy. 2012;10:8.
65. Nobs SP, Kayhan M, Kopf M. GM-CSF intrinsically controls eosinophil accumulation in the setting of allergic airway inflammation. J Allergy Clin Immunol. 2019;143:1513–1524.e2.
66. Molofsky AB et al. Interleukin-33 and interferon-γ counter-regulate group 2 innate lymphoid cell activation during immune perturbation. Immunity. 2015;43:161–174.
67. Gupta OT, Gupta RK. Visceral adipose tissue mesothelial cells: Living on the edge or just taking up space? Trends Endocrinol Metab 2015;26:515–523.
68. Braile M et al. Human lung-resident macrophages express and are targets of thymic stromal lymphopoietin in the tumor microenvironment. Cells. 2021;10:2012.
69. Kolter J et al. A subset of skin macrophages contributes to the surveillance and regeneration of local nerves. Immunity. 2019;50: 1482–1497.e7.

The Journal of Immunology, 2025, 00, 1–14
https://doi.org/10.1093/jimmun/vkae064
Research Article